

Coexistence of clean- and dirty-limit superconductivity in LiFeAs

Y. M. Dai,^{1,*} H. Miao,² L. Y. Xing,² X. C. Wang,² C. Q. Jin,^{2,3} H. Ding,^{2,3} and C. C. Homes^{1,†}

¹*Condensed Matter Physics and Materials Science Department, Brookhaven National Laboratory, Upton, New York 11973, USA*

²*Beijing National Laboratory for Condensed Matter Physics, Institute of Physics, Chinese Academy of Sciences, P.O. Box 603, Beijing 100190, China*

³*Collaborative Innovation Center of Quantum Matter, Beijing, China*

(Received 21 April 2015; revised manuscript received 22 December 2015; published 8 February 2016)

The optical properties of LiFeAs with $T_c \simeq 18$ K have been determined in the normal and superconducting states. The superposition of two Drude components yields a good description of the low-frequency optical response in the normal state. Below T_c , the optical conductivity reveals two isotropic superconducting gaps with $\Delta_1 \simeq 2.9 \pm 0.2$ meV and $\Delta_2 \simeq 5.5 \pm 0.4$ meV. A comparison between the superconducting-state Mattis-Bardeen and the normal-state Drude components, in combination with a spectral weight analysis, indicates that the spectral weight associated with a band which has a very small scattering rate is fully transferred to the superfluid weight upon the superconducting condensate. These observations provide clear evidence for the coexistence of clean- and dirty-limit superconductivity in LiFeAs.

DOI: [10.1103/PhysRevB.93.054508](https://doi.org/10.1103/PhysRevB.93.054508)

Iron-based superconductors (FeSCs) are multiband materials with multiple superconducting (SC) gaps opening on different Fermi surfaces in the superconducting state [1]. Understanding the properties of the SC gaps is an essential step towards describing the pairing mechanism. In FeSCs, superconductivity is generally achieved by suppressing the magnetic and structural transitions in the parent compounds [2] through chemical substitutions [3,4], which can introduce disorder. Strong disorder, in particular in-plane disorder, has been demonstrated to induce subgap absorption or pair-breaking effects in FeSCs [5–7]. As a result, the spectroscopic features of the SC gaps, as well as the values for $2\Delta/k_B T_c$ may be affected by excess impurity scattering [5,7] in doped materials. Furthermore, the overlap or interaction between superconductivity and the magnetic order may also complicate the measurement and analysis of the SC gaps in the underdoped regime.

LiFeAs presents an ideal system to clarify the properties of the SC gaps, as it is structurally simple and exhibits superconductivity with a relatively high critical temperature $T_c \simeq 18$ K in its stoichiometric form [8,9]. In the absence of disorder caused by chemical substitution, the nature of the SC gaps may be unambiguously determined by spectroscopic techniques. In addition, LiFeAs shows neither magnetic nor structural transitions [10–12], so that the superconducting properties are not affected by the coexistence or interaction with other ordered states.

Recent studies on LiFeAs using angle-resolved photoemission spectroscopy (ARPES) [13,14] and scanning tunneling microscopy (STM) [15,16] have revealed nodeless SC gaps with values in good agreement with each other: $\Delta_s = 2.5$ – 2.8 meV and $\Delta_l = 5.0$ – 6.0 meV. The presence of a large gap with $2\Delta_l/k_B T_c \gtrsim 6$ places this material, at least partially, in the strong-coupling limit. Having consistently established the properties of the SC gaps by surface-sensitive techniques [13–16], it is of the utmost importance to compare these

results with bulk-sensitive probes. The bulk values of the SC gaps derived from specific heat measurements ($\Delta_s = 1.2$ meV and $\Delta_l = 2.6$ meV) are only half of the values determined by ARPES and STM, placing LiFeAs entirely in the weak-coupling limit [17,18]. The specific heat by Wei *et al.* revealed an even smaller SC gap on the order of 0.7 meV [19]. An optical study on LiFeAs by Min *et al.* [20] reported two isotropic gaps with values larger than the ones from specific heat studies, yet still much smaller than ARPES and STM measurements; on the other hand, Lobo *et al.* [21] observed no clear-cut signature of the SC gap from their recent optical data, which they attribute to clean-limit superconductivity in LiFeAs. However, the existing optical data on LiFeAs seem to suffer from surface contamination due to the extremely air-sensitive nature of this compound, as evidenced by the unexpected noise or kinks in the reflectivity spectra accompanied by the suppression or smearing of the phonon features at 240 and 270 cm^{-1} . To resolve the existing contradictions, further experimental, especially optical, investigations into the SC gaps in LiFeAs crystals that are free of surface contamination is indispensable.

In this article, we have obtained the reflectivity of LiFeAs, which is characterized by sharp phonon lineshapes and a lack of any anomalous features, indicating the absence of surface contamination. We provide clear optical evidence for two nodeless SC gaps with values of $\Delta_1 \simeq 2.9 \pm 0.2$ meV and $\Delta_2 \simeq 5.5 \pm 0.4$ meV, consistent with ARPES and STM measurements. By comparing the superconducting-state Mattis-Bardeen with the normal-state Drude components, we find that a band with very small scattering rate disappears from the finite-frequency optical conductivity upon the formation of a superconducting condensate. A spectral weight analysis indicates that the spectral weight lost at finite frequency due to the formation of the superconducting condensate is fully recovered in the superfluid weight. Our experimental results suggest that superconducting bands in both the clean and dirty limits coexist in LiFeAs.

High-quality LiFeAs single crystals were grown by a self-flux method [22]. The T -dependent dc resistivity $\rho(T)$ of LiFeAs, as shown in the inset of Fig. 1, is characterized by a sharp superconducting transition at $T_c \simeq 18$ K. In the normal

*ymdai@lanl.gov

†homes@bnl.gov

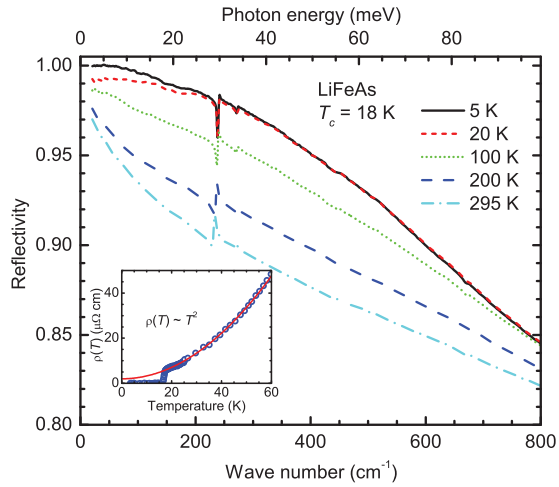


FIG. 1. Far-infrared reflectivity of LiFeAs at several temperatures above and below T_c . Inset: The dc resistivity as a function of temperature $\rho(T)$ in the low-temperature region (circles); the solid curve is the fit to $\rho(T) = \rho_0 + AT^2$.

state $\rho(T)$ follows a quadratic T dependence, $\rho(T) = \rho_0 + AT^2$ (ρ_0 is the residual resistivity), in the low-temperature region expected for a Fermi liquid, consistent with previous transport studies [23,24]. The residual resistivity of our crystal ($\rho_0 \approx 1.45 \mu\Omega \text{ cm}$) is quite small, leading to a very large residual-resistivity ratio (RRR) of $\rho(300 \text{ K})/\rho_0 \approx 200$. This indicates that the density of impurities or defects in LiFeAs is extremely low.

The experimental details about the reflectivity $R(\omega)$ measurements are described in the supplementary material [25]. Figure 1 shows the in-plane $R(\omega)$ of LiFeAs in the far-infrared region at several different temperatures. In the normal state, $R(\omega)$ approaches unity at zero frequency and increases with decreasing temperature in the far-infrared region, indicating a metallic response. Below T_c , at 5 K, an upturn in $R(\omega)$ develops at low frequency, which is a clear signature of the opening of a SC gap or gaps [26–29].

The real part of the optical conductivity, $\sigma_1(\omega)$, which provides direct information about the properties of the SC gaps [26–30], was determined from the Kramers-Kronig analysis of the reflectivity. Given the metallic nature of the LiFeAs material, in the normal state the Hagen-Rubens form $1 - R(\omega) \propto \omega^{-2}$ was used for the low-frequency extrapolation, while in the superconducting state $1 - R(\omega) \propto \omega^4$ was used. For the high-frequency extrapolation, we assumed a constant reflectivity above the highest-measured frequency up to 12.5 eV, followed by a free-electron response $R(\omega) \propto \omega^{-4}$.

Figure 2 displays $\sigma_1(\omega)$ for LiFeAs up to 800 cm^{-1} for different temperatures above and below T_c . The normal-state far-infrared $\sigma_1(\omega)$ exhibits a Drude-like metallic response, which may be described as a peak centered at zero frequency where the width of the Drude response at half maximum is the value of the quasiparticle scattering rate. As the temperature is reduced, the scattering rate decreases, resulting in a narrowing of the Drude peak. Just above T_c at 20 K, as shown by the short-dashed curve, the Drude peak is quite narrow, suggesting a very small quasiparticle scattering rate at low temperature. Upon entering the superconducting state, as shown by $\sigma_1(\omega)$

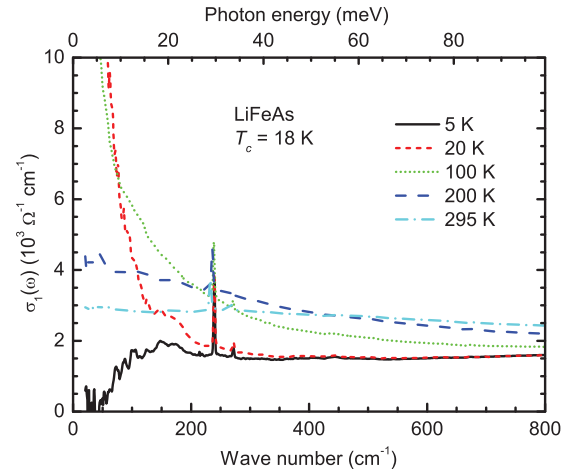


FIG. 2. The real part of the optical conductivity for LiFeAs in the far-infrared region at several temperatures above and below T_c .

at 5 K (solid curve), the low-frequency Drude-like response is no longer observed, and a dramatic suppression of $\sigma_1(\omega)$ at low frequency sets in, signaling the opening of the SC gaps. The conductivity almost vanishes below $\sim 50 \text{ cm}^{-1}$, suggesting the absence of nodes in the SC gaps, consistent with ARPES [13,14] and STM [15,16] as well as a previous optical study [20].

The normal-state $\sigma_1(\omega)$ of this multiband material is best described using the Drude-Lorentz model [31],

$$\sigma_1(\omega) = \frac{2\pi}{Z_0} \left[\sum_k \frac{\omega_{p,k}^2}{\tau_k(\omega^2 + \tau_k^{-2})} + \sum_j \frac{\gamma_j \omega^2 \Omega_j^2}{(\omega_j^2 - \omega^2)^2 + \gamma_j^2 \omega^2} \right], \quad (1)$$

where $Z_0 \simeq 377 \Omega$ is the vacuum impedance. The first term corresponds to a sum of free-carrier Drude responses where $\omega_{p,k}$ and $1/\tau_k$ are the plasma frequency and scattering rate in the k th intraband contribution, respectively; the second term describes a sum of Lorentz oscillators, with ω_j , γ_j , and Ω_j being the resonance frequency, width, and strength of the j th vibration or bound excitation. The solid curve in Fig. 3 is the experimental $\sigma_1(\omega)$ at 20 K, while the long-dashed line is the fit to the data; the fitted line consists of a narrow (coherent) Drude component with $\omega_{p,1} \simeq 8500 \pm 400 \text{ cm}^{-1}$ and $1/\tau_1 \simeq 27 \pm 3 \text{ cm}^{-1}$ (short-dashed line), a broad (incoherent) Drude component with $\omega_{p,2} \simeq 13000 \pm 500 \text{ cm}^{-1}$ and $1/\tau_2 \simeq 2200 \pm 150 \text{ cm}^{-1}$ (dash-dot line), along with several Lorentz oscillators (dotted line) that describe interband transitions [32] and infrared-active phonons. The inset of Fig. 3 displays the fitting result in the far-infrared region. This approach has been widely employed to describe the optical response of FeSCs [28,33–36].

Having modeled the normal-state optical response, we proceed to the analysis of the data below T_c . Generally, the superconducting-state $\sigma_1(\omega)$ is reproduced by introducing an isotropic superconducting energy gap on each of the Drude bands using a Mattis-Bardeen formalism (supplementary material [25]). As shown in Fig. 4(a), the linear superposition of two isotropic SC gaps [29,31,37,38] with the same (unchanged) Lorentz terms from the normal state yields a

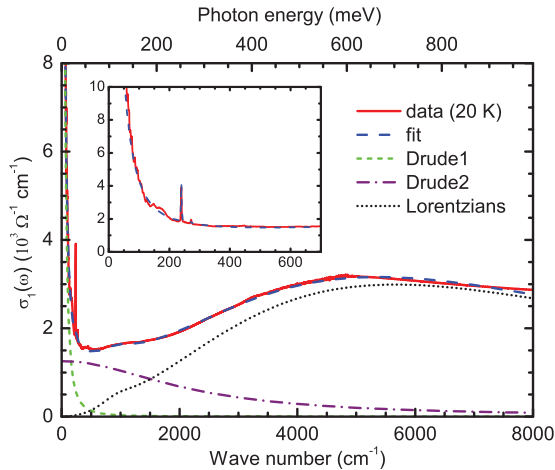


FIG. 3. The solid line shows the measured $\sigma_1(\omega)$ of LiFeAs up to 8000 cm^{-1} (1 meV) at 20 K . The long-dashed line through the data is the Drude-Lorentz fitting result, which consists of the contributions from a narrow Drude (short-dashed line), a broad Drude (long-dash-dot line), and a series of Lorentz components (dotted line). The inset displays $\sigma_1(\omega)$ (solid curve) and the fitting result (long-dashed line) in the low-frequency range.

very good fit to the experimental data at 5 K . The gap values determined from the fit are $\Delta_1 \simeq 2.9 \pm 0.2 \text{ meV}$ and $\Delta_2 \simeq 5.5 \pm 0.4 \text{ meV}$, respectively, in good agreement with the photoemission [13,14] and tunneling [15,16] studies; however, both are larger than a previous optical result on the same material [20]. The ratio of $2\Delta_1/k_B T_c \simeq 3.7$ for the small gap is consistent with the BCS weak-coupling limit of 3.5, whereas $2\Delta_2/k_B T_c \simeq 7.1$ for the large gap, pointing to strong-coupling superconductivity in LiFeAs. The coexistence of weak- and strong-coupling behaviors is likely to be a common feature in FeSCs.

Although the Mattis-Bardeen approach describes the superconducting-state $\sigma_1(\omega)$ quite well, and gives reasonable values for the SC gaps, we notice that while the plasma frequency of the broad Mattis-Bardeen component takes the same value as the corresponding normal-state Drude term ($\omega'_{p,2} = \omega_{p,2} \simeq 13000 \pm 500 \text{ cm}^{-1}$), the plasma frequency of the narrow Mattis-Bardeen ($\omega'_{p,1} \simeq 4500 \pm 200 \text{ cm}^{-1}$) is much smaller than the corresponding Drude term ($\omega_{p,1} \simeq 8500 \pm 400 \text{ cm}^{-1}$). Here we would like to point out that in our initial fit, the plasma frequencies for both Mattis-Bardeen terms adopt the values from the corresponding Drude terms ($\omega'_{p,1} = \omega_{p,1}$ and $\omega'_{p,2} = \omega_{p,2}$). However, in order to achieve a reasonable fit to the data, the plasma frequency for the narrow Mattis-Bardeen component $\omega'_{p,1}$ has to be reduced. This indicates that a band disappears from the finite frequency $\sigma_1(\omega)$ upon the superconducting condensate. More interestingly, the scattering rate of the narrow Mattis-Bardeen ($1/\tau'_1 = 128 \pm 8 \text{ cm}^{-1}$) becomes larger than the normal-state Drude component ($1/\tau_1 = 27 \pm 3 \text{ cm}^{-1}$). This is unusual, since the quasiparticle scattering rate usually decreases slightly in the superconducting state. However, if we take the disappeared band into account, this behavior can be well understood by considering that the normal-state Drude component with $1/\tau_1 = 27 \pm 3 \text{ cm}^{-1}$ indeed describes the momentum average

of a band with $1/\tau'_1 = 128 \pm 8 \text{ cm}^{-1}$ and another band with a very small scattering rate ($1/\tau''_1 \ll 27 \text{ cm}^{-1}$), which are strongly correlated with each other. Upon the formation of a superconducting condensate, the band with $1/\tau''_1 \ll 27 \text{ cm}^{-1}$ disappears from the finite-frequency $\sigma_1(\omega)$, so that only the band with $1/\tau'_1 = 128 \pm 8 \text{ cm}^{-1}$ can be observed in the superconducting state.

A spectral weight analysis provides clues about whether the disappeared band participates in the superconducting condensate. The spectral weight is defined as the area under $\sigma_1(\omega)$ over a given frequency interval,

$$N(\omega_c) = \int_{0^+}^{\omega_c} \sigma_1(\omega) d\omega, \quad (2)$$

where ω_c is a cut-off frequency. In the superconducting state, the low-frequency spectral weight is significantly suppressed due to the formation of the SC gaps. According to the Ferrell-Glover-Tinkham (FGT) sum rule [39,40], the spectral weight lost at finite frequencies in $\sigma_1(\omega)$ due to the superconducting condensate is transferred to the superfluid weight N_s ; this is precisely the superfluid density, which may be calculated from the imaginary part of the optical conductivity $\sigma_2(\omega)$ (see supplementary material [25]). The spectral weight lost at finite frequencies due to superconducting condensate $\Delta N(\omega_c)$, the so-called missing area, can be determined from a simple

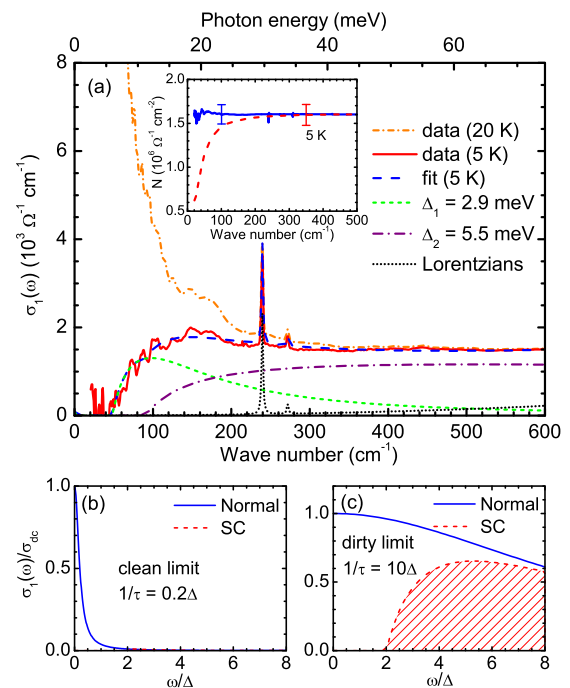


FIG. 4. (a) The short dash-dotted curve and the solid curve are the measured $\sigma_1(\omega)$ in the normal (20 K) and superconducting (5 K) states, respectively. The long dashed line through the data at 5 K denotes the calculated $\sigma_1(\omega)$ with two gaps of $\Delta_1 \simeq 2.9 \text{ meV}$ (short dashed line) and $\Delta_2 \simeq 5.5 \text{ meV}$ (long dash-dotted line). Inset: the superfluid weight N_s calculated from the imaginary part of the optical conductivity (solid line) and the missing area $\Delta N(\omega_c)$ (long-dashed line), respectively. Panels (b) and (c) illustrate the optical conductivity in the clean- and dirty-limit cases, respectively.

integral,

$$\Delta N(\omega_c) \simeq \int_{0^+}^{\omega_c} \sigma_1(\omega, 20 \text{ K}) - \sigma_1(\omega, 5 \text{ K}) d\omega. \quad (3)$$

The FGT sum rule requires that $\Delta N(\omega_c)$ is equal to N_s as long as ω_c covers the spectrum of excitations responsible for the superconducting condensate, regardless of the details of the system. N_s and $\Delta N(\omega_c)$ are shown as solid and dashed curves, respectively, in the inset of Fig. 4(a). N_s and $\Delta N(\omega_c)$ merge together above 350 cm^{-1} , suggesting that the spectral weight lost at finite frequencies in the superconducting state, including the spectral weight associated with the disappeared band, is fully captured by the superfluid weight located at zero frequency. The superfluid plasma frequency $\omega_{\text{ps}} \simeq 7822 \text{ cm}^{-1}$ is calculated from N_s via $\omega_{\text{ps}}^2 = Z_0 N_s / \pi^2$. The penetration depth $\lambda = 1/2\pi\omega_{\text{ps}}$ is $204 \pm 8 \text{ nm}$, which is smaller than the value from previous optical studies [20,21], but very close to the values from other techniques [11,41,42].

The above observations precisely reflect the optical response of a clean-limit superconducting band. A clean-limit superconductor is described as $l \gg \xi$, where $l \approx v_F \tau$ (v_F denotes the Fermi velocity) is the mean free path and $\xi \approx v_F / \Delta$ is the coherence length [43]. Hence, the clean-limit case is also given by $1/\tau \ll \Delta$ [Fig. 4(b)], indicating that nearly all of the spectral weight lies below 2Δ . Upon the superconducting condensate, almost all of the spectral weight collapses into the superfluid weight located at zero frequency, leaving no observable conductivity at finite frequency [hatched region in Fig. 4(b)]. Therefore, a clean-limit superconducting band disappears from the finite-frequency $\sigma_1(\omega)$ in the superconducting state due to the superconducting condensate, and the SC gap cannot be observed in the optical conductivity [44]. In the dirty limit [Fig. 4(c)], $1/\tau \geq \Delta$, meaning that a large portion of the spectral weight lies above 2Δ , which does not participate in the superconducting condensate below T_c . With a large part of spectral weight left at finite frequency in the superconducting state [hatched region in Fig. 4(c)], the SC gap can be clearly observed and accurately modeled by the Mattis-Bardeen formalism.

In LiFeAs, at least one band is in the clean limit, while others are in the dirty limit. The dirty-limit superconducting bands allow the SC gaps to be clearly observed from the optical conductivity and properly described by the Mattis-Bardeen approach, whereas the clean-limit superconducting band transfers almost all of its spectral weight to the zero-frequency superfluid weight below T_c , thus giving rise to the

disappeared band. Since the clean-limit condition is defined through a comparison of the quasiparticle scattering rate with the superconducting gap, clean- and dirty-limit superconductivity can only coexist in a *multiband superconductor* with *very small residual scattering rate* alongside *large and small superconducting gaps*. LiFeAs satisfies the above conditions simultaneously, thus supporting the coexistence of clean- and dirty-limit superconductivity.

The presence of clean-limit superconductivity in LiFeAs is favored by a number of experimental facts: (i) The residual resistivity of LiFeAs is very low: $\rho_0 \approx 1.45 \mu\Omega \text{ cm}$ for our sample, and $\rho_0 \approx 1.3 \mu\Omega \text{ cm}$ in a previous transport study [24], resulting in a mean free path as large as $l \approx 2000 \text{ \AA}$ at low temperature [24]. (ii) Upper critical field studies [45,46] have determined the *ab*-plane coherence length $\xi_{ab} \approx 40 \text{ \AA}$, which is much shorter than l , placing LiFeAs in the clean limit. (iii) An investigation into the vortex behavior in LiFeAs using STM [47] has revealed a T -dependent vortex-core radius, direct evidence of the Kramer-Pesch effect that is expected in a clean superconductor. (iv) Large superconducting gaps with $\Delta \approx 5$ and 4.2 meV have been observed by ARPES on the inner hole and one of the electron FSs [13], respectively, where the extracted quasiparticle scattering rates are extremely small (limited by the energy resolution) in the superconducting state [48].

To summarize, the optical properties of LiFeAs ($T_c \simeq 18 \text{ K}$) have been examined above and below T_c . Two isotropic SC gaps with $\Delta_1 \simeq 2.9 \pm 0.2 \text{ meV}$ and $\Delta_2 \simeq 5.5 \pm 0.4 \text{ meV}$ are determined from the superconducting-state optical conductivity. Interestingly, a band with a very small scattering rate vanishes from the finite-frequency optical conductivity in the superconducting state, as revealed by a comparison between the superconducting-state Mattis-Bardeen and normal-state Drude components. A spectral weight analysis demonstrates that the spectral weight associated with the disappeared band is fully recovered in the superfluid weight. These observations suggest the coexistence of clean- and dirty-limit superconductivity in LiFeAs.

We thank J. P. Hu, R. P. S. M. Lobo, and B. Xu for helpful discussions. Work at BNL was supported by the US Department of Energy, Office of Basic Energy Sciences, Division of Materials Sciences and Engineering under Contract No. DE-SC0012704. Work at IOP CAS was supported by NSFC (No. 11474344 and No. 11220101003) and MOST (No. 2013CB921703).

[1] H. Ding, P. Richard, K. Nakayama, K. Sugawara, T. Arakane, Y. Sekiba, A. Takayama, S. Souma, T. Sato, T. Takahashi *et al.*, *Europhys. Lett.* **83**, 47001 (2008).
 [2] M. Rotter, M. Tegel, D. Johrendt, I. Schellenberg, W. Hermes, and R. Pöttgen, *Phys. Rev. B* **78**, 020503 (2008).
 [3] M. Rotter, M. Tegel, and D. Johrendt, *Phys. Rev. Lett.* **101**, 107006 (2008).
 [4] A. S. Sefat, R. Jin, M. A. McGuire, B. C. Sales, D. J. Singh, and D. Mandrus, *Phys. Rev. Lett.* **101**, 117004 (2008).

[5] Y. Bang, H.-Y. Choi, and H. Won, *Phys. Rev. B* **79**, 054529 (2009).
 [6] R. P. S. M. Lobo, Y. M. Dai, U. Nagel, T. Rößler, J. P. Carbotte, T. Timusk, A. Forget, and D. Colson, *Phys. Rev. B* **82**, 100506(R) (2010).
 [7] M. L. Teague, G. K. Drayna, G. P. Lockhart, P. Cheng, B. Shen, H.-H. Wen, and N.-C. Yeh, *Phys. Rev. Lett.* **106**, 087004 (2011).
 [8] X. Wang, Q. Liu, Y. Lv, W. Gao, L. Yang, R. Yu, F. Li, and C. Jin, *Solid State Commun.* **148**, 538 (2008).

- [9] J. H. Tapp, Z. Tang, B. Lv, K. Sasmal, B. Lorenz, P. C. W. Chu, and A. M. Guloy, *Phys. Rev. B* **78**, 060505 (2008).
- [10] C. Chu, F. Chen, M. Gooch, A. Guloy, B. Lorenz, B. Lv, K. Sasmal, Z. Tang, J. Tapp, and Y. Xue, *Phys. C (Amsterdam, Neth.)* **469**, 326 (2009).
- [11] F. L. Pratt, P. J. Baker, S. J. Blundell, T. Lancaster, H. J. Lewtas, P. Adamson, M. J. Pitcher, D. R. Parker, and S. J. Clarke, *Phys. Rev. B* **79**, 052508 (2009).
- [12] N. Qureshi, P. Steffens, Y. Drees, A. C. Komarek, D. Lamago, Y. Sidis, L. Harnagea, H.-J. Grafe, S. Wurmehl, B. Büchner *et al.*, *Phys. Rev. Lett.* **108**, 117001 (2012).
- [13] K. Umezawa, Y. Li, H. Miao, K. Nakayama, Z.-H. Liu, P. Richard, T. Sato, J. B. He, D.-M. Wang, G. F. Chen *et al.*, *Phys. Rev. Lett.* **108**, 037002 (2012).
- [14] S. V. Borisenko, V. B. Zabolotnyy, A. A. Kordyuk, D. V. Evtushinsky, T. K. Kim, I. V. Morozov, R. Follath, and B. Büchner, *Symmetry* **4**, 251 (2012).
- [15] S. Chi, S. Grothe, R. Liang, P. Dosanjh, W. N. Hardy, S. A. Burke, D. A. Bonn, and Y. Pennec, *Phys. Rev. Lett.* **109**, 087002 (2012).
- [16] M. P. Allan, A. W. Rost, A. P. Mackenzie, Y. Xie, J. C. Davis, K. Kihou, C. H. Lee, A. Iyo, H. Eisaki, and T.-M. Chuang, *Science* **336**, 563 (2012).
- [17] U. Stockert, M. Abdel-Hafiez, D. V. Evtushinsky, V. B. Zabolotnyy, A. U. B. Wolter, S. Wurmehl, I. Morozov, R. Klingeler, S. V. Borisenko, and B. Büchner, *Phys. Rev. B* **83**, 224512 (2011).
- [18] D.-J. Jang, J. B. Hong, Y. S. Kwon, T. Park, K. Gofryk, F. Ronning, J. D. Thompson, and Y. Bang, *Phys. Rev. B* **85**, 180505 (2012).
- [19] F. Wei, F. Chen, K. Sasmal, B. Lv, Z. J. Tang, Y. Y. Xue, A. M. Guloy, and C. W. Chu, *Phys. Rev. B* **81**, 134527 (2010).
- [20] B. H. Min, J. B. Hong, J. H. Yun, T. Iizuka, S. Ichi Kimura, Y. Bang, and Y. S. Kwon, *New J. Phys.* **15**, 073029 (2013).
- [21] R. P. S. M. Lobo, G. Chanda, A. V. Pronin, J. Wosnitza, S. Kasahara, T. Shibauchi, and Y. Matsuda, *Phys. Rev. B* **91**, 174509 (2015).
- [22] L. Y. Xing, H. Miao, X. C. Wang, J. Ma, Q. Q. Liu, Z. Deng, H. Ding, and C. Q. Jin, *J. Phys. Condens. Matter* **26**, 435703 (2014).
- [23] O. Heyer, T. Lorenz, V. B. Zabolotnyy, D. V. Evtushinsky, S. V. Borisenko, I. Morozov, L. Harnagea, S. Wurmehl, C. Hess, and B. Büchner, *Phys. Rev. B* **84**, 064512 (2011).
- [24] F. Rullier-Albenque, D. Colson, A. Forget, and H. Alloul, *Phys. Rev. Lett.* **109**, 187005 (2012).
- [25] See Supplemental Material at <http://link.aps.org/supplemental/10.1103/PhysRevB.93.054508> for details of experimental methods and models for data analysis.
- [26] G. Li, W. Z. Hu, J. Dong, Z. Li, P. Zheng, G. F. Chen, J. L. Luo, and N. L. Wang, *Phys. Rev. Lett.* **101**, 107004 (2008).
- [27] K. W. Kim, M. Rössle, A. Dubroka, V. K. Malik, T. Wolf, and C. Bernhard, *Phys. Rev. B* **81**, 214508 (2010).
- [28] J. J. Tu, J. Li, W. Liu, A. Punnoose, Y. Gong, Y. H. Ren, L. J. Li, G. H. Cao, Z. A. Xu, and C. C. Homes, *Phys. Rev. B* **82**, 174509 (2010).
- [29] Y. M. Dai, B. Xu, B. Shen, H. H. Wen, X. G. Qiu, and R. P. S. M. Lobo, *Europhys. Lett.* **104**, 47006 (2013).
- [30] A. Charnukha, O. V. Dolgov, A. A. Golubov, Y. Matiks, D. L. Sun, C. T. Lin, B. Keimer, and A. V. Boris, *Phys. Rev. B* **84**, 174511 (2011).
- [31] D. Wu, N. Barišić, P. Kallina, A. Faridian, B. Gorshunov, N. Drichko, L. J. Li, X. Lin, G. H. Cao, Z. A. Xu *et al.*, *Phys. Rev. B* **81**, 100512 (2010).
- [32] P. Marsik, C. N. Wang, M. Rössle, M. Yazdi-Rizi, R. Schuster, K. W. Kim, A. Dubroka, D. Munzar, T. Wolf, X. H. Chen *et al.*, *Phys. Rev. B* **88**, 180508 (2013).
- [33] M. Nakajima, T. Tanaka, S. Ishida, K. Kihou, C. H. Lee, A. Iyo, T. Kakeshita, H. Eisaki, and S. Uchida, *Phys. Rev. B* **88**, 094501 (2013).
- [34] A. Charnukha, D. Pröpper, T. I. Larkin, D. L. Sun, Z. W. Li, C. T. Lin, T. Wolf, B. Keimer, and A. V. Boris, *Phys. Rev. B* **88**, 184511 (2013).
- [35] Y. M. Dai, B. Xu, B. Shen, H. Xiao, H. H. Wen, X. G. Qiu, C. C. Homes, and R. P. S. M. Lobo, *Phys. Rev. Lett.* **111**, 117001 (2013).
- [36] M. Nakajima, S. Ishida, T. Tanaka, K. Kihou, Y. Tomioka, T. Saito, C. H. Lee, H. Fukazawa, Y. Kohori, T. Kakeshita *et al.*, *Sci. Rep.* **4**, 5873 (2014).
- [37] M. Nakajima, S. Ishida, K. Kihou, Y. Tomioka, T. Ito, Y. Yoshida, C. H. Lee, H. Kito, A. Iyo, H. Eisaki *et al.*, *Phys. Rev. B* **81**, 104528 (2010).
- [38] C. C. Homes, A. Akrap, J. S. Wen, Z. J. Xu, Z. W. Lin, Q. Li, and G. D. Gu, *Phys. Rev. B* **81**, 180508 (2010).
- [39] R. E. Glover and M. Tinkham, *Phys. Rev.* **104**, 844 (1956).
- [40] M. Tinkham and R. A. Ferrell, *Phys. Rev. Lett.* **2**, 331 (1959).
- [41] D. S. Inosov, J. S. White, D. V. Evtushinsky, I. V. Morozov, A. Cameron, U. Stockert, V. B. Zabolotnyy, T. K. Kim, A. A. Kordyuk, S. V. Borisenko *et al.*, *Phys. Rev. Lett.* **104**, 187001 (2010).
- [42] H. Kim, M. A. Tanatar, Y. J. Song, Y. S. Kwon, and R. Prozorov, *Phys. Rev. B* **83**, 100502 (2011).
- [43] M. Dressel and G. Grüner, *Electrodynamics of Solids* (Cambridge University Press, Cambridge, UK, 2002).
- [44] K. Kamarás, S. L. Herr, C. D. Porter, N. Tache, D. B. Tanner, S. Etemad, T. Venkatesan, E. Chase, A. Inam, X. D. Wu *et al.*, *Phys. Rev. Lett.* **64**, 84 (1990).
- [45] B. Lee, S. Khim, J. S. Kim, G. R. Stewart, and K. H. Kim, *Europhys. Lett.* **91**, 67002 (2010).
- [46] S. Khim, B. Lee, J. W. Kim, E. S. Choi, G. R. Stewart, and K. H. Kim, *Phys. Rev. B* **84**, 104502 (2011).
- [47] T. Hanaguri, K. Kitagawa, K. Matsubayashi, Y. Mazaki, Y. Uwatoko, and H. Takagi, *Phys. Rev. B* **85**, 214505 (2012).
- [48] H. Miao, T. Qian, X. Shi, P. Richard, T. K. Kim, M. Hoesch, L. Y. Xing, X.-C. Wang, C.-Q. Jin, J.-P. Hu *et al.*, *Nat. Commun.* **6**, 6056 (2015).